Supporting Information

Achieving highly selective CO_2 adsorption on SAPO-35 zeolites by template-modulating the framework silicon content

Yan Li,[a,†] Hongwei Chen,[b,†] Chaoran Wang,[a] Yu Ye,[a] Libo Li,[b] Xiaowei Song*[a] and Jihong Yu*[a,c]

[a] State Key Laboratory of Inorganic Synthesis and Preparative Chemistry, College of Chemistry, Jilin University, 2699 Qianjin Street, Changchun 130012, P.R. China

[b] College of Chemical Engineering and Technology, Shanxi Key Laboratory of Gas Energy Efficient and Clean Utilization, Taiyuan University of Technology, Taiyuan 030024, P.R. China

[c] International Center of Future Science, Jilin University, 2699 Qianjin Street, Changchun 130012, P.R. China

*Corresponding Authors. † These authors contributed equally.

E–mail addresses: xiaoweisong@jlu.edu.cn, jihong@jlu.edu.cn

This Supporting Information Includes:

Details for experiments, characterizations and calculations

Tables S1-S8

Figures S1-S11

Experimental Details

Materials

Tetraethyl orthosilicate (TEOS, 28 wt.%, Tianjin Fuchen Chemical Reagents Company), phosphoric acid (H_3PO_4, 85 wt.%, Beijing Chemical Works), boehmite (Catapal B, Al_2O_3, 72.7 wt.%, Sasol), N-methylpiperidine (NMP, 99%, J&K Scientific LTD), and deionized water were used in the following syntheses. All the chemicals and reagents were purchased from commercial sources and used without purification.

Synthetic procedures

In a typical synthesis, 0.50 g boehmite was dispersed in 8 mL of H_2O and 1.66 g H_3PO_4 with stirring for 1 h. Then, TEOS (0.15, 0.45 and 1.05 g) was slowly added, and the resulting mixture was stirred for another 3 h. Afterwards, 2.70 mL of NMP was added, and the mixture was stirred for another 2 h. The gel was transferred into a 15 mL Teflon-lined stainless-steel autoclave and heated at 180 °C for 3 days under static conditions. The obtained products were separated by centrifuging with deionized water for 3 times and dried overnight at 100 °C, followed by calcination at 600 °C for 6 h at the heating rate of 1 °C/min in air. The obtained samples were labeled as SAPO-35_*x*, wherein *x* represents Si contents, i.e., Si/(Si+P+Al) in molar ratio depended on the addition of TEOS measured by inductively coupled plasma atomic emission spectra (ICP-AES).

Characterizations

The crystallinity and phase purity of the samples were characterized by powder X-ray diffraction (PXRD) on a Rigaku diffractometer equipped with a graphite monochromator using Cu Kα radiation (λ = 1.5418 Å) operated at 50 kV and 200 mA in steps of 0.02 °. The crystal size and morphology were measured by scanning electron microscope (SEM) on a JSM-6700F. Ammonium temperature-programmed desorption (NH_3-TPD) profiles were measured by Autochem II 2920 on an apparatus equipped with an electric conductivity device as a detector. Chemical composition was determined with inductively coupled plasma atomic emission spectra (ICP-AES) analyses carried out on a PerkinElmer Optima 3300DV spectrometer. Solid-state ^{29}Si MAS NMR experiments were performed on Bruker Avance Neo 600Mz WB spectrometer with BBO MAS probe operating at a magnetic field strength of 14.1 T (Bruker Company, Karlsruhe, Germany). Single component equilibrium adsorption isotherms for Nitrogen (N_2) at 77 K were performed on Micromeritics ASAP 2020 instrument. Carbon dioxide (CO_2) at 273, 283 and 298 K and N_2 at 273, 298 K adsorption data

were collected from the Micromeritics 3-Flex. Before each measurement, all the samples were degassed at 623 K for 8 h under vacuum (P/P_0 = 10^{-5}) to desorb all adsorbed gases and water. Adsorption isotherms were then acquired at the corresponding temperatures, which were controlled by condensation pump and Dewar flask with the fluctuations less than ±0.2 K during the experiments. The breakthrough experiments for CO_2/N_2 mixtures were carried out at a flow rate of 3 mL/min (298 K, 100 kPa) on Agilent GC490 equipment. Prior to the breakthrough experiment, the sample was firstly activated at 623 K for 8 h at the activation station. After activation, the sample was loaded in the glove box (oxygen isolation) at room temperature. Activated sample was packed into a self-made adsorption column (inner diameter 10 mm and length 115 mm, adsorbent mass 5.7985 g) stainless steel column under pure N_2 atmosphere. Connect the adsorption column with the test device, then the dehydration sample was loaded and further activated in situ by flushing the adsorption bed with helium gas for 2 h at 523 K at a flow rate of 30 mL/min. Under helium gas purge, CO_2 on the adsorbent can be removed well, and the adsorption column was cleaned by He purge to realize the recycling of the adsorbent. The breakthrough experiments in moist condition were then carried out with the relative humidity of ~40% by employing a vapor generator to generate the moisture at 298 K and 1 bar.

Calculations of the Isosteric Heats of Gas Adsorption (Q_{st}):

The isosteric heats (Q_{st}) of adsorption for SAPO-35_0.08, SAPO-35_0.14 and SAPO-35_0.22 were calculated by fitting the CO_2 adsorption isotherms measured at 273 K, 283 K and 298 K to the Virial equation.[1]

$$\ln P = \ln N + {}^{1}/_{T}\sum_{i=0}^{m} a_i N^i + \sum_{j=0}^{n} b_j N^j \qquad (1)$$

$$Q_{st} = -R\sum_{i=0}^{m} a_i N^i \qquad (2)$$

N: amount adsorbed (mg/g);

P: pressure (mmHg);

T: temperature (K);

a_i, b_j: constants;

R: 8.314 J·mol^{-1}·K^{-1}

Prediction of adsorption of binary mixture by IAST theory

In order to perform the IAST calculations, the single-component isotherm was fitted by the dual-site Langmuir-Freundlich (DSLF) adsorption model to correlate the pure-component equilibrium data and further to predict the adsorption of mixtures.[2] The DSLF model is described as:

$$q = q_{m_1} \times \frac{b_1 \times p^{1/n_1}}{1 + b_1 \times p^{1/n_1}} + q_{m_2} \times \frac{b_2 \times p^{1/n_2}}{1 + b_2 \times p^{1/n_2}} \quad (3)$$

Where p is the fugacity of bulk gas at equilibrium with adsorbed phase, q_{m1} and q_{m2} are the model parameters of the maximum adsorption amount, b_1 and b_2 are the affinity constants. n_1 and n_2 are the deviations from an ideal homogeneous surface.

Based on the above model parameters of pure gas adsorption, we used the IAST model, which was proposed by Myer and Prausnitz in 1965 to predict the multi-component adsorption.[3] Analogous to Raoult's law for vapor-liquid equilibrium, the IAST assumes that the adsorbed solutions are ideal and all activity coefficients in the adsorbed phase are unity. Thus, the adsorption equilibrium between adsorbed and gas phases will lead to the following equation

$$P y_i \varphi_i = x_i f_i^0(\pi) \quad (4)$$

Where f_i^0 is the fugacity of the equilibrium gas phase corresponding to the spreading pressure π for the adsorption of pure gas i, φ_i is the gas fugacity coefficient of component i calculated by *PR* equation of state, and x_i and y_i are the molar fraction of component i at the adsorbed and bulk phases, respectively. The binary gas mixing process is carried out at constant spreading pressure π and indicated by

$$\int_0^{f_1^0} b_1^0(f_1) d\ln(f_1) = \int_0^{f_2^0} b_2^0(f_2) d\ln(f_2) \quad (5)$$

Where the single-component adsorption amount and selectivity are further obtained from the above equation by numerical integration and root exploration. To investigate the separation of binary mixtures, the adsorption selectivity is defined by

$$S_{ij} = \frac{x_i / x_j}{y_i / y_j} \quad (6)$$

Where the selectivity refers to the first component over the second one, and the x_i, x_j and y_i, y_j, denote the molar fractions of species i, j in the adsorbed and bulk phases, respectively.

Table S1. Framework compositions and textural properties of SAPO-35_*x* samples.

No.	Samples	Molar Composition[a]	S_{BET}[b] (m^2/g)	S_{micro}[c] (m^2/g)	V_{micro}[c] (cm^3/g)	V_{total}[d] (cm^3/g)
1	SAPO-35_0.08	$Si_{0.08}Al_{0.50}P_{0.42}O_2$	493	455	0.22	0.23
2	SAPO-35_0.14	$Si_{0.14}Al_{0.48}P_{0.38}O_2$	502	469	0.22	0.24
3	SAPO-35_0.22	$Si_{0.22}Al_{0.44}P_{0.34}O_2$	447	382	0.18	0.21

[a] Measured by inductively coupled plasma atomic emission spectra (ICP-AES). [b] S_{BET} surface area calculated by applying the BET equation over the pressure range 0.05-0.30 P/P_0. [c] S_{micro} (micropore area) and V_{micro} (micropore volume) calculated using the t-plot method over the pressure range 0.08-0.25 P/P_0. [d] V_{total} (total pore volume) calculated at $P/P_0 = 0.995$.

Table S2. Reported CO_2 adsorption capacities for other AlPO zeolites and SAPO zeolites in comparison with SAPO-35_0.14.

Material name	Topology	Condition	CO_2 capacity (mmol/g)	Ref.
SAPO-35_0.14	**LEV**	273 K, 100 kPa	4.8	This work
AlPO-14	**AFN**	273 K, 100 kPa	2.7	[4]
AlPO-17	**ERI**	273 K, 100 kPa	2.3	[5]
AlPO-18	**AEI**	273 K, 100 kPa	2.1	
AlPO-25	**ATV**	273 K, 100 kPa	1.1	
AlPO-53	**AEN**	273 K, 100 kPa	1.9	
AlPO-11	**AEL**	298 K, 100 kPa	0.8	[6]
SAPO-17	**ERI**	298 K, 100 kPa	1.7	[7]
SAPO-43	**GIS**	298 K, 100 kPa	1.1	[8]
SAPO-56	**AFX**	273 K, 100 kPa	5.5	[9]
SAPO-**CHA**	**CHA**	273 K, 100 kPa	3.6	
SAPO-17	**ERI**	273 K, 100 kPa	3.3	
SAPO-35	**LEV**	273 K, 100 kPa	3.6	
SAPO-34	**CHA**	298 K, 100 kPa	2.8	[10]
SAPO-DNL-6	**RHO**	298 K, 100 kPa	4.7	[11]
SAPO-**RHO**	**RHO**	298 K, 100 kPa	4.4	[12]

Table S3. Size and electronic properties of CO_2 and N_2.

Gas	Kinetic diameter (nm)	Polarizability (10^{-25} cm^3)[13]	Quadruple moment (10^{-40} C m^2)[13]
CO_2	0.33	26.3	13.4
N_2	0.36	17.7	4.7

Table S4. Fitting parameters of DSLF adsorption model for SAPO-35_0.08.

Parameters	CO_2 at 273 K	CO_2 at 298 K	N_2 at 273 K	N_2 at 298 K
q_{m1} (mmol/g)	0.13989	3.8824	26.76647	6.62244
q_{m2} (mmol/g)	5.30738	0.58362	0.92203	26.83334
b_1 (kPa^{-1})	0.34308	0.01502	5.05999E-8	3.13096E-4
b_2 (kPa^{-1})	0.04196	0.08819	0.00526	2.69219E-18
$1/n_1$	1.33457	0.92319	2.46453	1.0126
$1/n_2$	0.85808	0.98501	1.06706	7.07073
R^2	0.99999	0.99999	0.99998	0.99992

Table S5. Fitting parameters of DSLF adsorption model for SAPO-35_0.14.

Parameters	CO_2 at 273 K	CO_2 at 298 K	N_2 at 273 K	N_2 at 298 K
q_{m1} (mmol/g)	3.199	4.81091	99.99973	0.05819
q_{m2} (mmol/g)	3.97987	1.53714	0.37385	25.80845
b_1 (kPa^{-1})	0.11294	0.00895	2.35855E-6	0.01575
b_2 (kPa^{-1})	0.0206	0.08292	0.01156	2.79964E-5
$1/n_1$	0.86032	0.9602	1.48836	1.13799
$1/n_2$	0.8459	0.94318	1.04823	1.17087
R^2	0.99999	1	0.99999	0.99989

Table S6. Fitting parameters of DSLF adsorption model for SAPO-35_0.22.

Parameters	CO_2 at 273 K	CO_2 at 298 K	N_2 at 273 K	N_2 at 298 K
q_{m1} (mmol/g)	0.08717	4.55709	0.53451	0.22161
q_{m2} (mmol/g)	5.35856	0.69242	14.76766	10
b_1 (kPa^{-1})	0.49762	0.01113	0.01052	0.01141
b_2 (kPa^{-1})	0.04397	0.08065	6.73E-6	1.533E-6
$1/n_1$	1.67063	0.93593	1.02954	1.08205
$1/n_2$	0.86372	0.99162	1.71521	2.00839
R^2	1	1	0.99999	0.99997

Table S7. Reported CO_2 adsorption capacity and CO_2/N_2 selectivities for other zeolites and adsorbing materials as compared with SAPO-35_0.14 (Si contents in relevant SAPOs are given in square brackets).

Material name	CO_2 capacity		CO_2/N_2		Ref.
	Condition	Uptake (mmol/g)	Condition	Selectivity	
SAPO-35_0.14 [0.14]	298 K, 100 kPa	3.4	298 K, 100 kPa (0.2:0.8)	49.9	This work
SAPO-43 [0.19]	298 K, 100 kPa	1.1	298 K, 100 kPa	15.28	[8]
SAPO-56 [0.15]	273 K, 100 kPa	5.5	273 K, 100 kPa	10.5	[9]
SAPO-**CHA** [0.11]	273 K, 100 kPa	3.6	273 K, 100 kPa	25.8	[9]
SAPO-17 [0.14]	273 K, 100 kPa	3.3	273 K, 100 kPa	8.7	[9]
SAPO-35 [0.08]	273 K, 100 kPa	3.6	273 K, 100 kPa	8.2	[9]
SAPO-DNL-6 [0.18]	298 K, 100 kPa	4.7	298 K, 100 kPa	19.5	[11]
SAPO-**RHO** [0.18]	298 K, 100 kPa	4.4	298 K, 100 kPa	50	[12]
Na-SAPO-RHO [0.18]	298 K, 100 kPa	3.5	298 K, 100 kPa	196	[12]
K-SAPO-RHO [0.18]	298 K, 100 kPa	0.9	298 K, 100 kPa	29	[12]
Cs-SAPO-RHO [0.18]	298 K, 100 kPa	0.5	298 K, 100 kPa	22	[12]
H-SSZ-13	298 K, 100 kPa	3.98	298 K, 100 kPa (0.15:0.85)	73.6	[13]
Cu-SSZ-13	298 K, 100 kPa	3.75	298 K, 100 kPa (0.15:0.85)	72	[13]

Co(II)/SSZ-13	298 K, 100 kPa	2.9	298 K, 100 kPa (0.15:0.85)	40.04	[14]
Ni(II)/SSZ-13	298 K, 100 kPa	3.0	298 K, 100 kPa (0.15:0.85)	38.67	[14]
SSZ-45	303 K, 100 kPa	0.5	303 K, 100 kPa (0.15:0.85)	24.3	[15]
Fe-**MOR**	298 K, 100 kPa	3.89	298 K, 100 kPa (0.15:0.85)	51.8	[16]
K-**CHA** (Si/Al = 1.9)	303 K, 100 kPa	1.5	303 K, 100 kPa (0.5:0.5)	90	[17]
Ca-**KFI**	303 K, 100 kPa	4.0	303 K, 100 kPa	70	[18]
Mg-**KFI**	303 K, 100 kPa	4.4	303 K, 100 kPa	98	[18]
NaKA (17 at.% K^+)	298 K, 85 kPa	3.43	298 K, 85 kPa	172	[19]
13X	298 K, 100 kPa	1.7	298 K, 100 kPa (0.5:0.5)	187	[20]
ZIF-8	298 K, 100 kPa	0.8	298 K, 100 kPa (0.5:0.5)	12.5	[20]
BPL activated carbon	298 K, 100 kPa	2.2	298 K, 100 kPa (0.5:0.5)	25	[20]
SBA-15	298 K, 100 kPa	3.5	298 K, 100 kPa	14.0	[21]
MCM-41	298 K, 100 kPa	0.7	298 K, 100 kPa (0.2:0.8)	11	[22]
mmen-CuBTTri	298 K, 100 kPa	4.0	298 K, 100 kPa (0.15:0.85)	165	[23]
SIFSIX-2-Cu-i	298 K, 100 kPa	5.1	298 K, 100 kPa (0.1:0.9)	140	[24]

Table S8. Comparison of CO_2 uptake and CO_2/N_2 IAST selectivity for SAPO-35_HMI and SAPO-35_0.14 at 273 K.

Samples	CO_2 at 100 kPa (mmol/g)	CO_2/N_2 at 273 K and 100 kPa	
		0.5: 0.5	0.2: 0.8
SAPO-35_0.14	4.76	25.1	40.4
SAPO-35_HMI	4.34	22.2	32.4

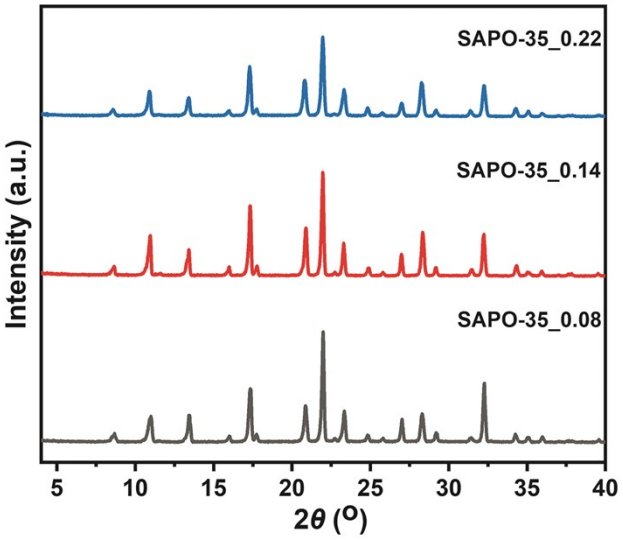

Fig. S1 PXRD patterns of SAPO-35_*x* samples.

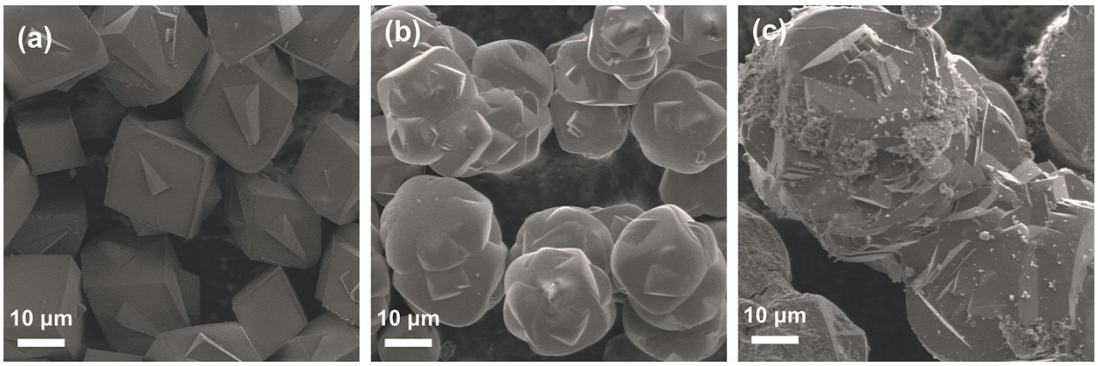

Fig. S2 SEM images of (a) SAPO-35_0.08, (b) SAPO-35_0.14, and (c) SAPO-35_0.22.

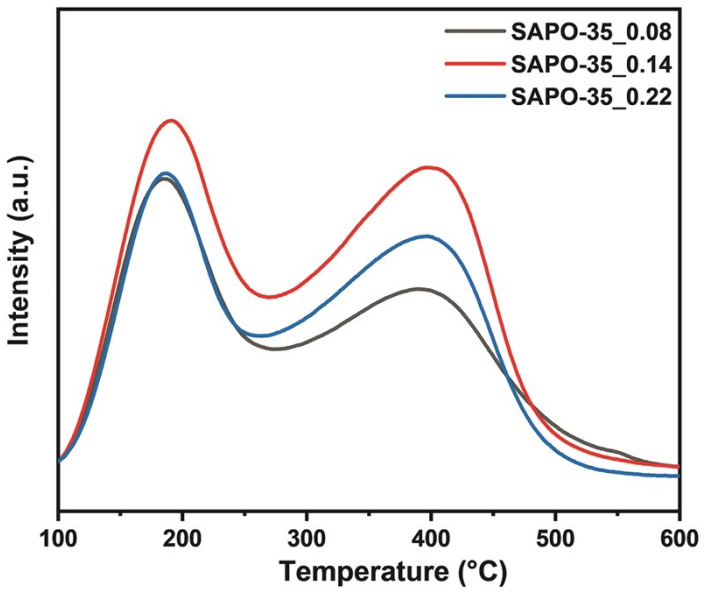

Fig. S3 NH_3-TPD profiles of SAPO-35_*x* samples.

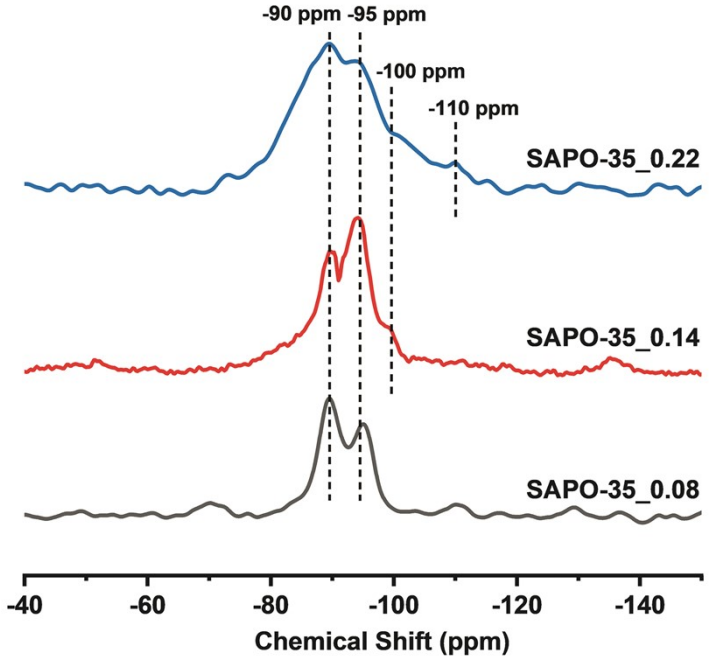

Fig. S4 [29] Si MAS NMR spectra of SAPO-35_*x* samples.

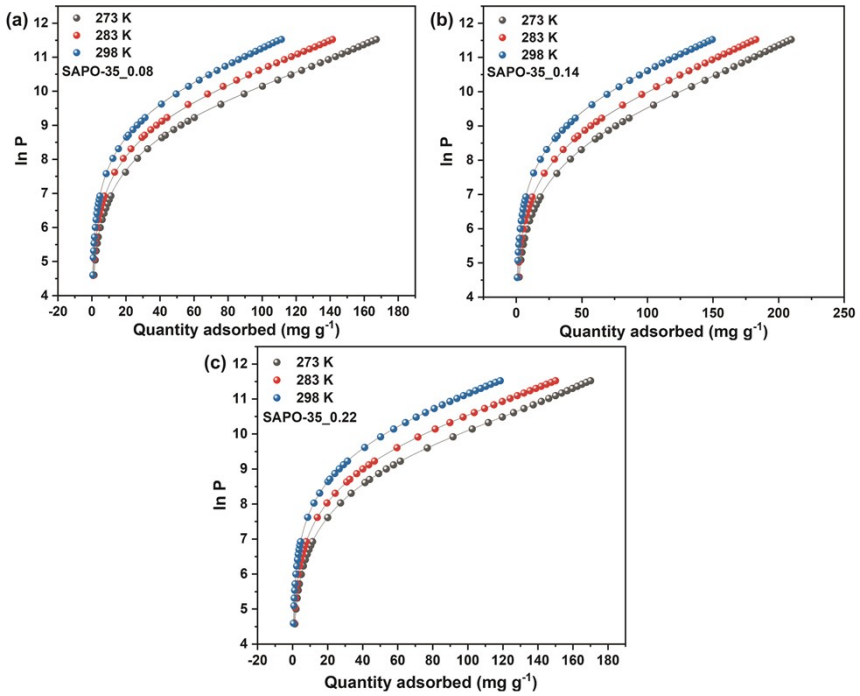

Fig. S5 Virial fittings for CO_2 isotherms of (a) SAPO-35_0.08, (b) SAPO-35_0.14, and (c) SAPO-35_0.22 at 273, 283 and 298 K.

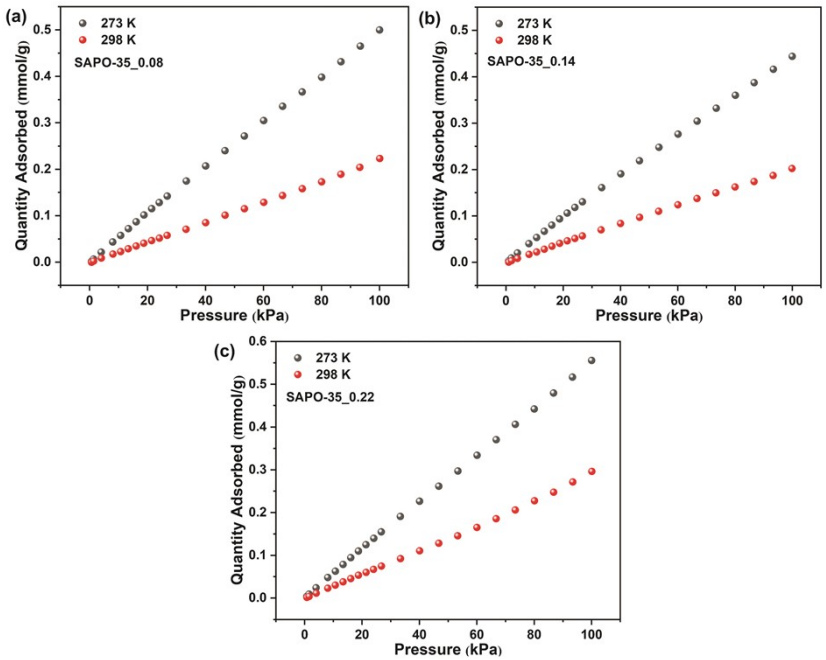

Fig. S6 N_2 adsorption of (a) SAPO-35_0.08, (b) SAPO-35_0.14, and (c) SAPO-35_0.22 at 273 K and 298 K.

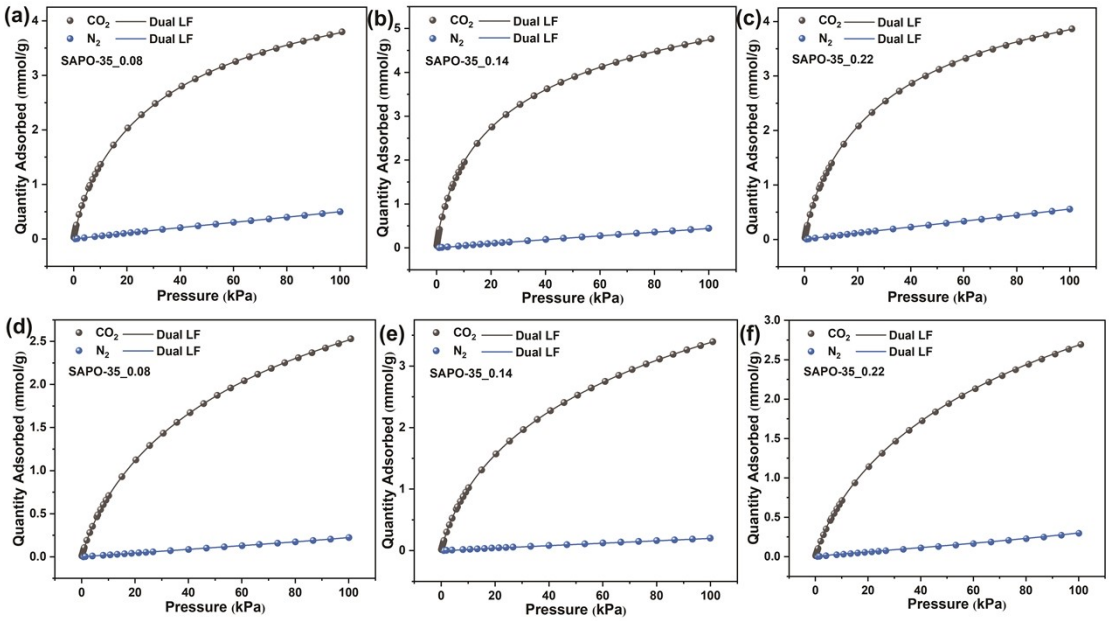

Fig. S7 CO_2 and N_2 gas adsorption isotherms for (a) SAPO-35_0.08, (b) SAPO-35_0.14, and (c) SAPO-35_0.22 at 273 K and (d) SAPO-35_0.08, (e) SAPO-35_0.14, and (f) SAPO-35_0.22 at 298 K.

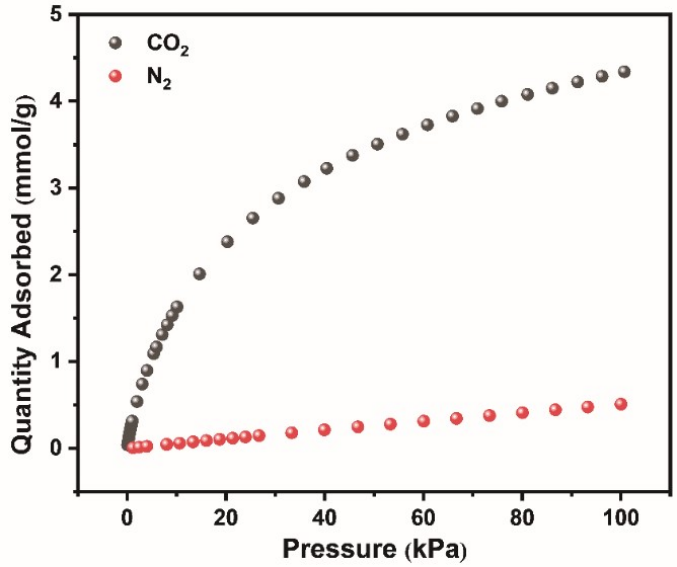

Fig. S8 CO_2 adsorption and N_2 adsorption of SAPO-35_HMI at 273 K.

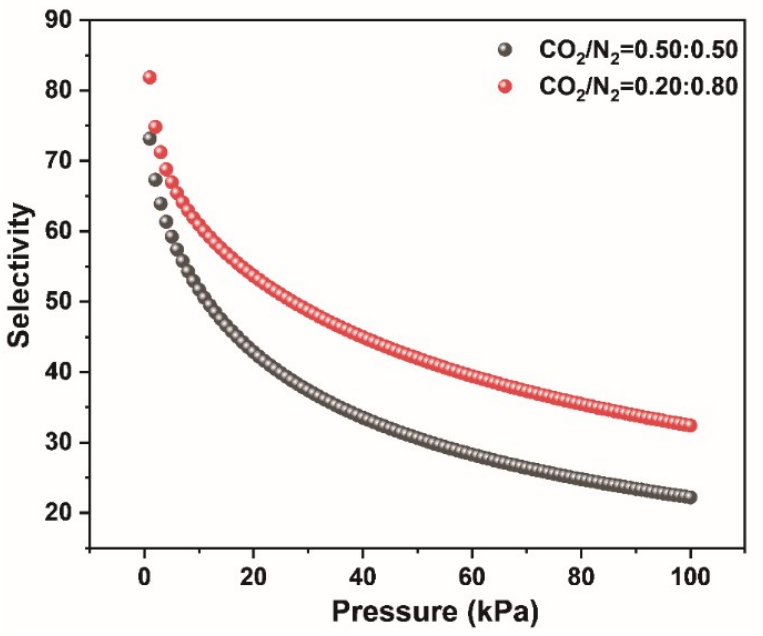

Fig. S9 CO_2/N_2 IAST selectivity for SAPO-35_HMI at 273 K.

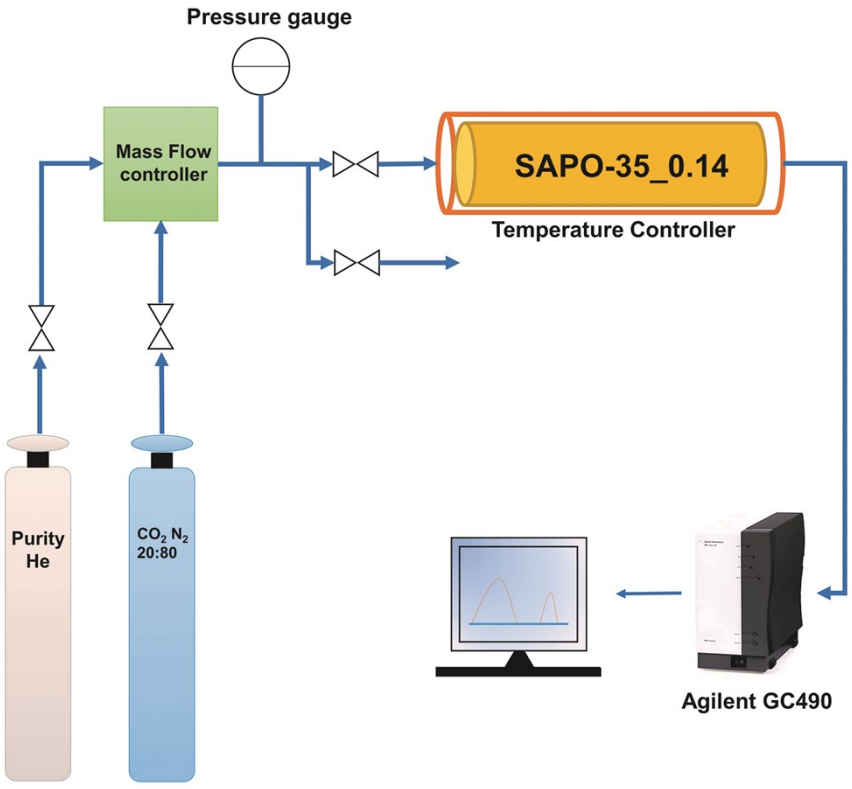

Fig. S10 The setup for the breakthrough experiments.

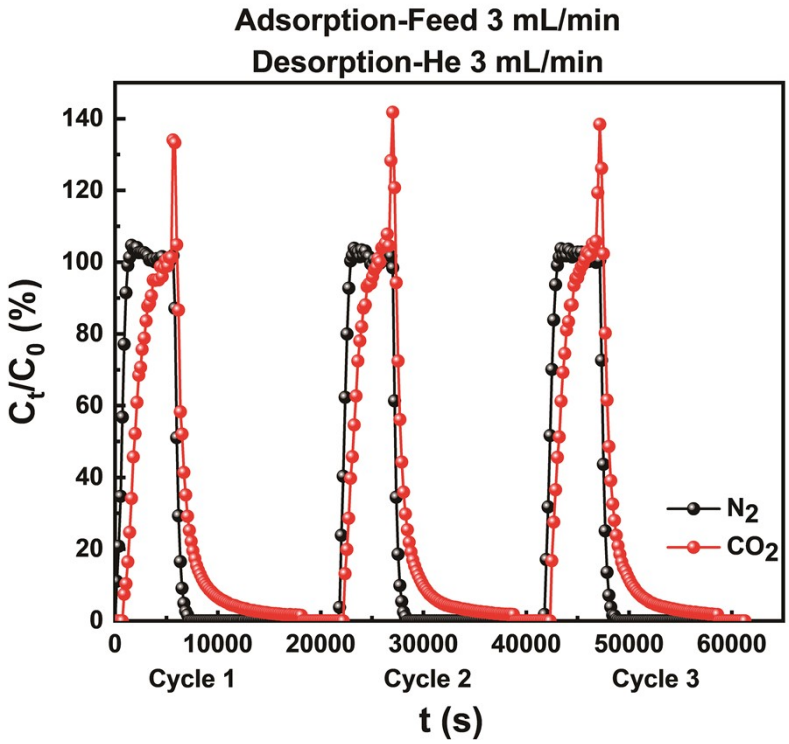

Fig. S11 Multiple consecutive cycles of breakthrough curves for SAPO-35_0.14 with the adsorption/desorption gas flow rate of 3 mL/min (CO_2/N_2 20:80 v/v, humidity 40%) at 298 K and atmospheric pressure. C_t and C_0 denotes outlet and inlet concentration, respectively.

References

1. M. Thommes, K. Kaneko, A. V. Neimark, J. P. Olivier, F. Rodriguez-Reinoso, J. Rouquerol and K. S. W. Sing, *Pure Appl. Chem.*, 2015, **87**, 1051-1069.
2. D. M. Ruthven, *Principles of adsorption and adsorption processes, Wiley: New York,* 1984.
3. A. L. Myers and J. M. Prausnitz, *AIChE. J.*, 1965, **11**, 121-127.
4. X. X. Zhao, X. L. Xu, L. B. Sun, L. L. Zhang and X. Q. Liu, *Energy Fuels*, 2009, **23**, 1534-1538.
5. Q. Liu, N. C. O. Cheung, A. E. Garcia-Bennett and N. Hedin, *ChemSusChem*, 2011, **4**, 91-97.
6. J. A. Delgado, V. I. Águeda, M. A. Uguina, J. L. Sotelo and P. Fernández, *Adsorption*, 2013, **19**, 407-422.
7. S. Zhong, N. Bu, R. Zhou, W. Jin, M. Yu and S. Li, *J. Membr. Sci.*, 2016, **520**, 507-514.
8. A. J. Hernández-Maldonado, R. T. Yang, D. Chinn and C. L. Munson, *Langmuir*, 2003, **19**, 2193-2200.
9. O. Cheung, Q. Liu, Z. Bacsik and N. Hedin, *Microporous Mesoporous Mater.*, 2012, **156**, 90-96.
10. J. Gong, C. Wang, C. Zeng and L. Zhang, *Microporous Mesoporous Mater.*, 2016, **221**, 128-136.
11. X. Su, P. Tian, D. Fan, Q. Xia, Y. Yang, S. Xu, L. Zhang, Y. Zhang, D. Wang and Z. Liu, *ChemSusChem*, 2013, **6**, 911-918.
12. X. Wang, N. Yan, M. Xie, P. Liu, P. Bai, H. Su, B. Wang, Y. Wang, L. Li, T. Cheng, P. Guo, W. Yan and J. Yu, *Chem. Sci.*, 2021, **12**, 8803-8810.
13. M. R. Hudson, W. L. Queen, J. A. Mason, D. W. Fickel, R. F. Lobo and C. M. Brown, *J. Am. Chem. Soc.*, 2012, **134**, 1970-1973.
14. M. Sun, Q. Gu, A. Hanif, T. Wang and J. Shang, *Chem. Eng. J.*, 2019, **370**, 1450-1458.
15. S. Smeets, D. Xie, L. B. McCusker, C. Baerlocher, S. I. Zones, J. A. Thompson, H. S. Lacheen and H.-M. Huang, *Chem. Mater.*, 2014, **26**, 3909-3913.
16. Y. Zhou, J. Zhang, L. Wang, X. Cui, X. Liu, S. S. Wong, H. An, N. Yan, J. Xie and C. Yu, *Science*, 2021, **373**, 315-320.
17. T. Du, X. Fang, L. Liu, J. Shang, B. Zhang, Y. Wei, H. Gong, S. Rahman, E. F. May and P. A. Webley, *Chem. Commun.*, 2018, **54**, 3134-3137.
18. Q. Liu, T. Pham, M. D. Porosoff and R. F. Lobo, *ChemSusChem*, 2012, **5**, 2237-2242.
19. Q. Liu, A. Mace, Z. Bacsik, J. Sun, A. Laaksonen and N. Hedin, *Chem. Commun.*, 2010, **46**, 4502-4504.
20. J. McEwen, J.-D. Hayman and A. Ozgur Yazaydin, *Chem. Phys.*, 2013, **412**, 72-76.
21. X. Liu, L. Zhou, X. Fu, Y. Sun, W. Su and Y. Zhou, *Chem. Eng. Sci.*, 2007, **62**, 1101-1110.
22. Y. Belmabkhout and A. Sayari, *Chem. Eng. Sci.*, 2009, **64**, 3729-3735.
23. T. M. McDonald, D. M. D'Alessandro, R. Krishna and J. R. Long, *Chem. Sci.*, 2011, **2**, 2022-2028.
24. P. Nugent, Y. Belmabkhout, S. D. Burd, A. J. Cairns, R. Luebke, K. Forrest, T. Pham, S. Ma, B. Space and L. Wojtas, *Nature*, 2013, **495**, 80-84.